Check for updates

Intra- and intermolecular-interaction-controlled reversible core–shell structures and photoluminescent properties of lanthanide ion-doped diblock copolymers†

Feifei Xue,[ab] Hongfei Li[*a] and Shichun Jiang [ID] [*ab]

Lanthanide-based nanotechniques continue to attract considerable attention due to their current range of applications and broad potential in optical devices and biomedicine. Lanthanide ion-loaded block copolymers (BCPs) have gained interest, with questions remaining regarding their luminescence properties and structures. Solutions and films containing polystyrene-*block*-poly(2-vinylpyridine) (S2VP) and polystyrene-*block*-poly(4-vinylpyridine) (S4VP) loaded with trivalent lanthanide ions (Ln^{3+} = Eu^{3+}, Tb^{3+}) were prepared using a solvent displacement method and spin coating approach. Atomic force microscopy and transmission electron microscopy observations confirmed the Ln^{3+} distribution in the core of S2VP [Ln(x)] micelles and the corona of S4VP[Ln(x)] micelles. The coordination of Ln^{3+} and the S2VP core segment led to micelle shrinkage and film dewetting with increasing Ln^{3+} concentration, while the coordination of Ln^{3+} and the S4VP corona chain swelled the micelle. Photoluminescence investigations of the complex solutions showed typical reddish (Eu^{3+}) and greenish (Tb^{3+}) luminescence, and the emission intensity was enhanced with increasing Ln^{3+} concentration without typical fluorescence concentration quenching behavior. The luminescence intensity was distinctly enhanced when Ln^{3+} was distributed in the micellar core. Moreover, the emission spectra of mixed Eu–Tb ions complexes gave addition spectra of the two separated complexes. An orange color emission was observed because Eu^{3+} was more emissive. These results would improve understanding of ion coordination and lay the foundation for lanthanide ion/BCPs complex applications.

Introduction

Block copolymers (BCPs) are of broad interest in current research across macromolecular chemistry and physics, ranging from the development of new synthetic strategies and molecular architectures to applications of advanced theoretical and computational methods.[1] Almost 50 years after the preparation of the first laboratory samples, scientific interest in BCPs continues to grow, not only regarding the properties of their components, but also the particular doping, spatial extent, connectivity, and orientation of their nanodomains. To further explore the novel properties of BCPs and develop their performance, attention has recently been focused on ion/BCP complexes. The added ions strongly affect the thermodynamic, structural, and other properties of ion/BCP complexes,

and advanced material with prominent performance can be obtained by selectively choosing ions.[2–5]

Trivalent lanthanide ions (Ln^{3+}) show excellent luminescent characteristics, including high color purity, high fluorescence intensity, and long fluorescence lifetime.[6–8] In particular, europium (Eu^{3+}) and terbium (Tb^{3+}) ions, which can emit red and green primary light colors, respectively, have drawn much attention due to their potential application in full color displays. Unfortunately, the direct absorption of lanthanide ions is very weak due to the parity forbidden nature of the 4f transitions. In past years, efforts have been made to overcome these disadvantages by incorporating Ln^{3+} ions into small molecules, sol–gel precursors, and polymers.[9–13] Compared with conventional luminescent materials, lanthanide complexes show excellent mechanical and electronic properties, thermal and chemical stability, biocompatibility, and hydrophobic–hydrophilic balance, while the luminescence features of lanthanide (Ln^{3+}) complexes show high photoluminescence efficiency with a narrow emission spectrum, a large Stokes shifts, and a long fluorescent lifetime. These features offer excellent prospects for the design of new luminescent materials with enhanced desired characteristics

[a] State Key Laboratory of Polymer Physics and Chemistry, Changchun Institute of Applied Chemistry, Chinese Academy of Sciences, Changchun 130022, P. R. China. E-mail: hfli@ciac.ac.cn

[b] School of Materials Science and Engineering, Tianjin University, Tianjin 300072, P. R. China. E-mail: scjiang@tju.edu.cn

and high added value for specific targeted applications. This opens exciting new directions in materials science and related technologies, with noteworthy results for the ecofriendly integration, miniaturization, and multifunctionalization of devices, among others.

In addition to traditional polymers, recent efforts have been made towards lanthanide ion/BCP complexes, especially lanthanide-containing block copolymer micelles.[14–17] Amphiphilic BCPs readily undergo microphase separation in selective solvents to form micelles with coronas of the soluble block and cores of the insoluble block, affording the opportunity to achieve discrete nanostructures through a spontaneous process. When such micelles are coordinated by lanthanide ions and transferred on to substrates by spin coating or dip coating, they arrange themselves in 2D arrays spontaneously. Meanwhile, the micellar structure not only provides a confined environment for the lanthanides, to prevent aggregation and reduce vibrational radiationless deactivation, but can also potentially shield the quenching effect. By flexibly controlling the type of lanthanide ions, ion concentration, micelle size, and the inter-micelle spacing, micellar thin films allow potential applications in biological fluorescent labeling, film technology, and more. Therefore, both the influence of lanthanide ions on the thermodynamic and structural properties of the BCP micellar thin films and the influence of BCPs on the luminescent characteristics of lanthanide ions are worth investigating.

Herein, a typical pair of BCPs, polystyrene-*block*-poly(2-vinylpyridine) (S2VP) and polystyrene-*block*-poly(4-vinylpyridine) (S4VP), were chosen. The pyridine rings in S2VP and S4VP can form strong coordination bonds with lanthanide ions. Although the only difference between these BCPs is the position of nitrogen in the pyridine ring (*ortho vs. para* positions), their dipole polarization and Flory–Huggins interaction parameter with polystyrene (PS) are totally different.[18–20] Using careful solvent selection, S2VP and S4VP might form opposite micelle structures in the same solvent, meaning that the lanthanide ions are associated with different micelle positions. In this article, by mixing lanthanide ions (Eu^{3+} or Tb^{3+}) with S2VP and S4VP, the influence of ion distribution (ion loading position) and ion concentration on luminescence features, and the short- and long-range structures of the complex films were investigated and discussed.

Experimental section

Materials

Symmetric S4VP ($M_{n,PS} = 22\,000$ g mol^{-1}, $M_{n,P4VP} = 22\,000$ g mol^{-1}, polydispersity index = 1.09) and S2VP ($M_{n,PS} = 40\,500$ g mol^{-1}, $M_{n,P2VP} = 40\,000$ g mol^{-1}, polydispersity index = 1.10) diblock copolymers were purchased from Polymer Source and used as received. Europium oxide (99.99%), terbium oxide (99.9%), and 1,10-phenanthroline (Phen) were obtained from Aldrich and stored in a desiccator. All solvents were analytical grade and used without further purification.

Preparation of lanthanide ion/BCP complexes

S2VP and S4VP were dissolved in a mixed solvent of anhydrous ethanol and *N,N*-dimethylformamide (DMF) (2 : 1, w/w), and stirred for 5 h to yield a 3 mg mL^{-1} solution. LnCl$_3$ (EuCl$_3$ or TbCl$_3$) solutions were prepared using the following steps: lanthanide oxides (Eu$_2$O$_3$ or Tb$_4$O$_7$) and excess hydrochloric acid aqueous solution (6 mol L^{-1}) were mixed with stirring. After the solid was completely dissolved, the solution was distilled at 50 °C until the formation of LnCl$_3 \cdot$6H$_2$O as white crystals. The crystals were dried under vacuum at 40 °C for 24 h, and then dissolved with anhydrous ethanol to give a 0.1 mol L^{-1} solution. Phen was dissolved in anhydrous ethanol (20 mg mL^{-1}).

Lanthanide ion/BCP complexes were prepared by mixing the LnCl$_3$, block copolymer, and Phen solutions. LnCl$_3$ solution was added dropwise to block copolymer solution, which was stirred for over 24 h at room temperature to obtain homogeneity. After 24 h, Phen solution was added dropwise to the mixed solution in a Phen/VP molar ratio of 3 : 2, and stirring was continued for 6 h. The resultant samples were denoted as S4VP[Eu(*x*)], S4VP[Tb(*x*)], S2VP[Eu(*x*)], and S4VP[Tb(*x*)], where *x* represents the loading molar ratios of lanthanide ions to pyridine units ($x = n_{Ln^{3+}}/n_{VP} = 0, 0.3, 0.5, 1.0$).

Characterization

The surface topography of thin films on silicon wafers was imaged using atomic force microscopy (AFM) (SPI3800N, Seiko Instruments Inc., Japan) in tapping mode. Cantilevers for AFM measurements with a spring constant of around 2 N m^{-1} were purchased from Olympus (Tokyo, Japan). Silicon wafers were diced into ~1 cm^2 pieces and cleaned successively in an ultra-sonic bath (acetone), "piranha" bath (concentrated H$_2$SO$_4$ and 30% H$_2$O$_2$ (70 : 30, v/v) at 90 °C), and deionized water, and then blown dry with nitrogen. Films on the cleaned wafer were fabricated by spin-coating.

Transmission electron microscopy (TEM; JEOL-2000) was used to study the nanostructures of the film samples. Samples were obtained by dropping the product solution onto a copper grid for TEM.

Dynamic light-scattering (DLS) measurements were performed on aqueous solutions with a Malvern Zetasizer Nano S (Malvern Instruments, Ltd.) equipped with a 4 mW He–Ne laser light operating at $\lambda = 633$ nm. All samples were kept at 25 °C with a scattering angle of 173°.

Fourier-transform infrared (FTIR) spectra were recorded on a Bruker Vertex 70 spectrometer.

Ultraviolet-visible (UV-vis) absorption spectra of the block copolymers and their lanthanide complexes were recorded on a TU-1901 spectrophotometer between 200 and 600 nm at room temperature.

Photoluminescence (PL) measurements were performed at room temperature using an F-280 spectrophotometer with a scanning rate of 1200 nm min^{-1} at room temperature. The slit widths for both excitation and emission were set at 5 nm.

Emission images of the rare earth complex samples, including powder, solution, and film samples, were taken under a 365 nm UV lamp at room temperature.

Results and discussion

Lanthanide ion distribution in BCP micelles

For diblock copolymers in specific solvent systems, the solubility difference between two blocks makes one block expand and the other collapse, yielding micelles. Fig. 1(a) and (b) show atomic force microscopy (AFM) images of thin films prepared from neat S4VP and S2VP solutions, in which the samples present typical dimple-type patterns, revealing the dried and partially collapsed spherical micellar structure. The micro-structures of these micelles were further analyzed by transmission electron microscopy (TEM) (shown in the insets of Fig. 1(a) and (b)). The TEM images presented characteristic core–corona structures with P4VP or P2VP blocks appearing as dark regions due to selective staining with iodine. It could be concluded that, in the binary solvent used here, S4VP and S2VP tended to form opposite micellar structures, with S4VP forming micelles with corona P4VP and core PS, and S2VP forming
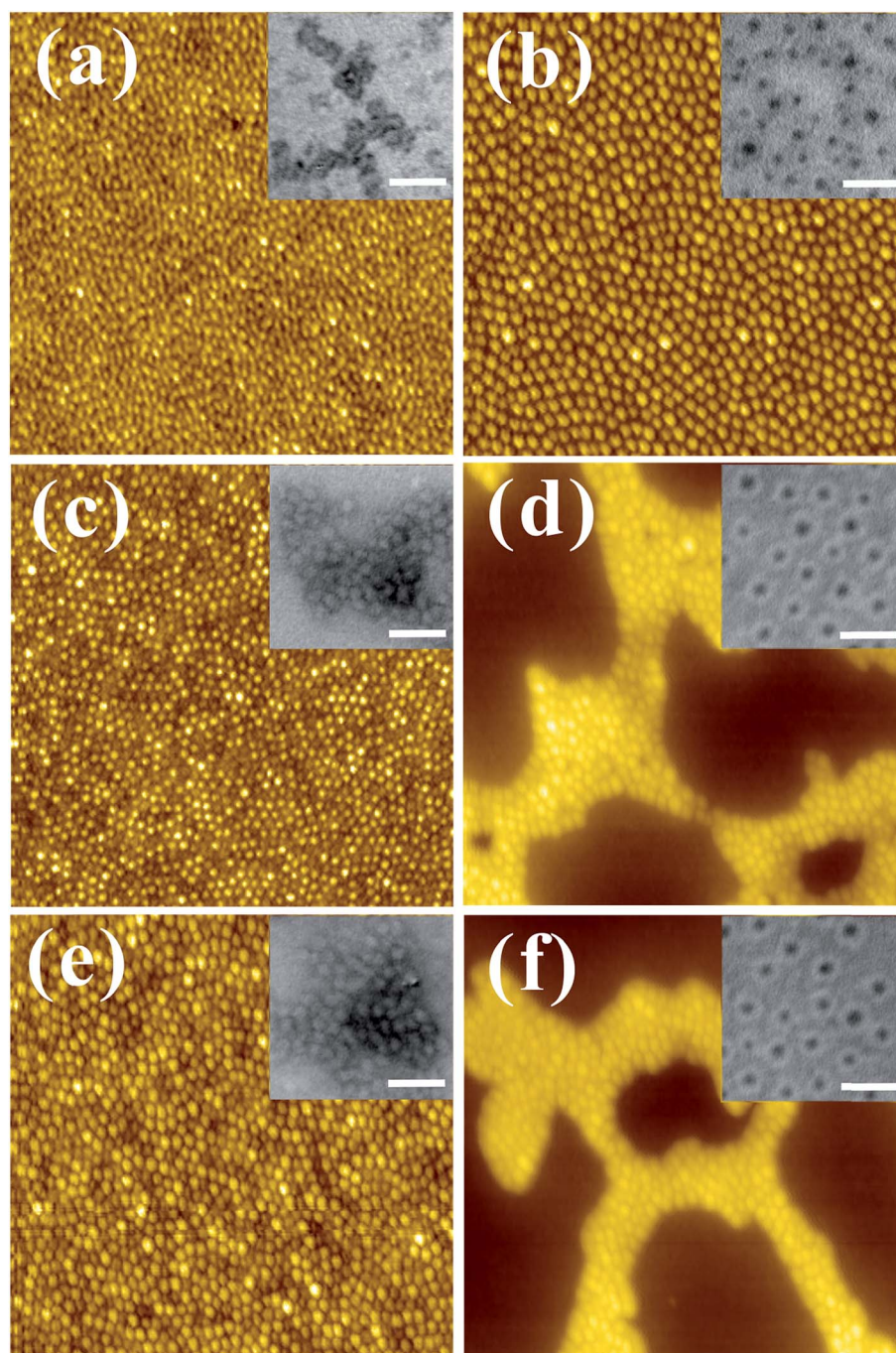

Fig. 1 AFM topography images (1 μm × 1 μm) of (a) S4VP, (b) S2VP, (c) S4VP[Eu(0.5)], (d) S2VP[Eu(0.5)], (e) S4VP[Tb(0.5)], and (f) S2VP[Tb(0.5)]. Insets are corresponding TEM photographs. Scale bar is 100 nm.

micelles with corona PS and core P2VP. These opposite micelle structures can be explained by the preferential affinities for the solvent. For S2VP, the affinity of the block for the solvent can be estimated from the solubility parameters of S2VP and solvent due to the weak polarity of the P2VP block. The solubility parameters (δ) of PS, P2VP, and the mixed solvent (ethanol/DMF) were 18.5, 20.4, and 13.0 ($\delta_{ethanol}$ = 13.4, δ_{DMF} = 12.1), respectively.[21,22] Obviously, the mixed solvent had a preferential affinity for the PS block, inducing a corona PS/core P2VP structure. In contrast, although the only difference between P4VP and P2VP was the nitrogen position in the pyridine ring (*ortho vs. para* positions), the dipole polarization of P4VP was much greater than that of P2VP. Therefore, the effect of polar interactions between S4VP and solvent on the resultant structure was large. As a result, the P4VP block tended to form the corona due to its strong interactions with ethanol in the solution.[23]

When Ln^{3+} ions were added to the micelle solutions, Ln^{3+} synchronously coordinated with the corresponding P4VP or P2VP segments due to interactions between Ln^{3+} and the pyridine ring. Fig. 1(c–f) show the morphologies of thin films prepared from S4VP[Eu(0.5)], S4VP[Tb(0.5)], S2VP[Eu(0.5)], and S2VP[Tb(0.5)] solutions. All samples present micellar structures, with no significant aggregation of Ln^{3+} was found in these hybrids, indicating a uniform dispersion of Ln^{3+} within the PVP microdomains. Meanwhile, the opposite micelle structure displayed the same results but with a different distribution of Ln^{3+} in the micelles, with Ln^{3+} loaded in the core of S2VP[Ln(x)] micelle and in the corona of S4VP[Ln(x)] micelle, respectively. Scheme 1 describes the Ln^{3+} distribution in BCP micelles through preferential coordination of the PVP chains and lanthanide ions.

FTIR spectroscopy provided insight into the coordination interactions between S4VP or S2VP and lanthanide ions. Fig. 2 shows the FTIR spectra of S2VP, S2VP–Eu, and S2VP–Tb. The characteristic pyridine ring peaks of S2VP at 1588 cm^{-1} ($\nu_{C=C+C=N}$) and 1559 cm^{-1} ($\nu_{C=N}$) were shifted to 1590 cm^{-1} and 1569 cm^{-1} in S2VP–Eu, and 1592 cm^{-1} and 1570 cm^{-1} in S2VP–Tb, respectively. Furthermore, the vibration peaks for –CH$_2$– in the S2VP copolymer at 2920 cm^{-1} ($\nu_{asC–H}$) and 2851 cm^{-1} ($\nu_{sC–H}$) also appeared in the spectra of the complexes. This demonstrated that coordination bonds had formed between Ln^{3+} and N in the 2VP segments of S2VP and that the backbone structure of the copolymer remained in the complex. P2VP blocks showed a rich basic Lewis base character, with the nitrogen atom incorporated within the aromatic ring tending to share a free-electron pair with the empty f orbitals of Ln^{3+}, causing changes in the electron distributions of those peaks related to the pyridine ring stretching modes. Similar spectral shifts were also observed in S4VP and its complexes (Fig. SI-1, ESI†).
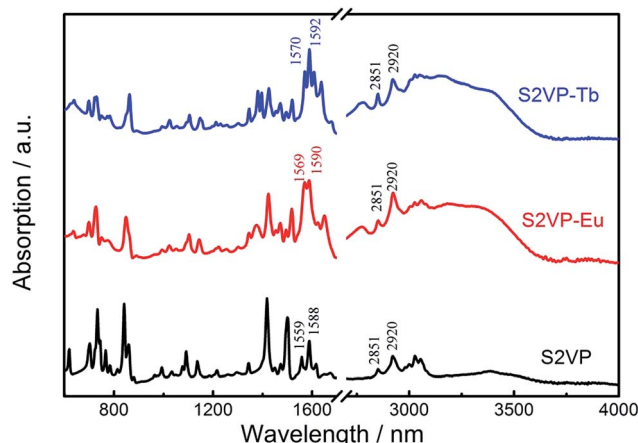

Fig. 2 FTIR spectra of S2VP, S2VP–Eu, and S2VP–Tb.

Dependence of micelle size on lanthanide concentration

Different Ln^{3+} distributions might result in distinct thermodynamic behaviors in short- and long-range structures. For instance, the sizes of S4VP[Ln(x)] and S2VP[Ln(x)] micelles showed the opposite trend with increasing Ln^{3+} loading ratio (x), with S4VP[Ln(x)] micelle size increasing monotonically with increasing x, while S2VP[Ln(x)] micelle size decreased (Fig. 3).

In general, the morphology and size of the micelles are mainly controlled by three factors, namely the extension of the core blocks, surface tension between the core and solvent, and repulsion among the corona chains.[24,25] Concerning the S4VP[Ln(x)] micelles, the corona chains were charged with Ln^{3+}, resulting in repulsive interactions among the charged corona, which generally involve a steric contribution, a solvation contribution, and an electrostatic repulsive contribution.[22,23] With increasing Ln^{3+} concentration, the overall charge better compensated the charge of unoccupied pyridine groups and reduced the electrostatic repulsion. Therefore, the interchain repulsive interactions between corona chains became weaker, causing an increase in micelle size to decrease the interfacial energy between the core and solvent. In the S2VP[Ln(x)] micelles, Ln^{3+} formed interactions with P2VP segments within the micelle core. As only steric–solvation interactions existed in nonionic corona chains, the introduction of Ln^{3+} mainly affected the extension of the core segments. With increasing Ln^{3+} concentration, the S2VP[Ln(x)] micelle diameter tended to decrease. We speculated that this was driven by multi-coordinate sites of Ln^{3+} and the P2VP block (each P2VP block might associate with many Ln^{3+} ions, and *vice versa*). This attraction between Ln^{3+} and the 2VP groups pulled them together, shrinking the micelle and increasing the micelle density. Therefore, we concluded that the Ln^{3+} distribution was crucial to determining micelle size evolution.

Dewetting phenomena

The stability of the as-spun Ln^{3+} associated S2VP films was affected by a form of dewetting, which we examined in detail AFM. All Ln^{3+} doped S2VP-films were dewetted to different

Scheme 1 Schematic illustration of Ln^{3+} distribution in BCP micelles through preferential coordination of PVP chains to lanthanide ions.
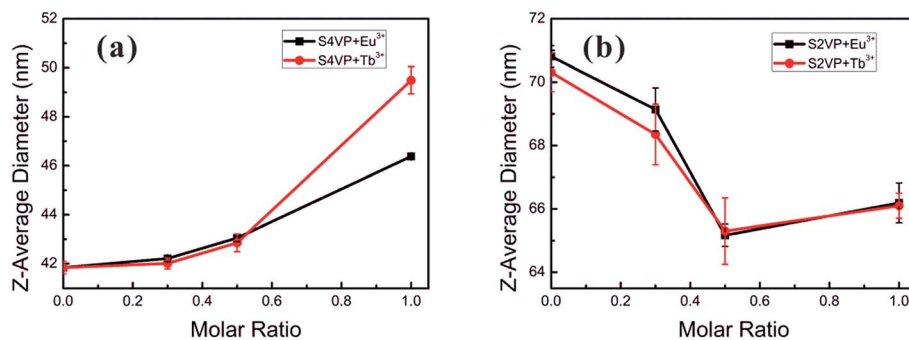
Fig. 3 Micelle size of (a) S4VP[Ln(x)] and (b) S2VP[Ln(x)] with increasing the Ln^{3+} concentration (molar ratio of Ln^{3+} ranging from 0 to 1.0).

extents during the spin coating process (Fig. 4), while films obtained from neat S2VP solution were homogeneous (Fig. SI-2, ESI†). Examining the featureless regions of the dewetted holes using AFM cross-section profiles gave an average thickness of about 5 nm (Fig. SI-3†). This suggested the existence of an adsorbed brush layer, with P2VP/Ln^{3+} acting as a wetting layer on the polar substrate and a PS layer of lower interfacial energy on top.[26–28] In contrast, the films of S4VP[Ln(x)] were homogeneous throughout the Ln^{3+} concentration range (Fig. SI-4†). Based on the above results, we speculated that these distinct behaviors in film stability originated from the different Ln^{3+} distributions.

The wetting of a solid surface by a polymer film appears to be result from the combination of short-range intermolecular interactions between polymer and substrate, and long-range dispersive van der Waals forces. According to the literature, two major forms of polymer dewetting have been highlighted.[27] In this scenario, as stated above, a layer of non-anchored S2VP [Ln(x)] micelles only partially wetted a monolayer of chemically identical molecules (a monolayer of S2VP[Ln(x)] complexes anchored on substrate), indicating that the relaxation of the thin films followed an autophobic dewetting mechanism.[29–35] At the non-wettable interface, the PS corona of micelles autophobically dewetted from a brush of PS blocks, which was analogous to dewetting of a PS homopolymer melt on top of a PS homopolymer brush.[36,37] Concerning the driving force, two main factors should be accounted for. Firstly, autophobic dewetting is believed to be primarily driven by entropy, which means that the conformation of the polymer brush layer contacting the substrate is different from that of the other polymer layers. With Ln^{3+} doping, the interactions between the ion doped P2VP and substrate are much stronger, leading to
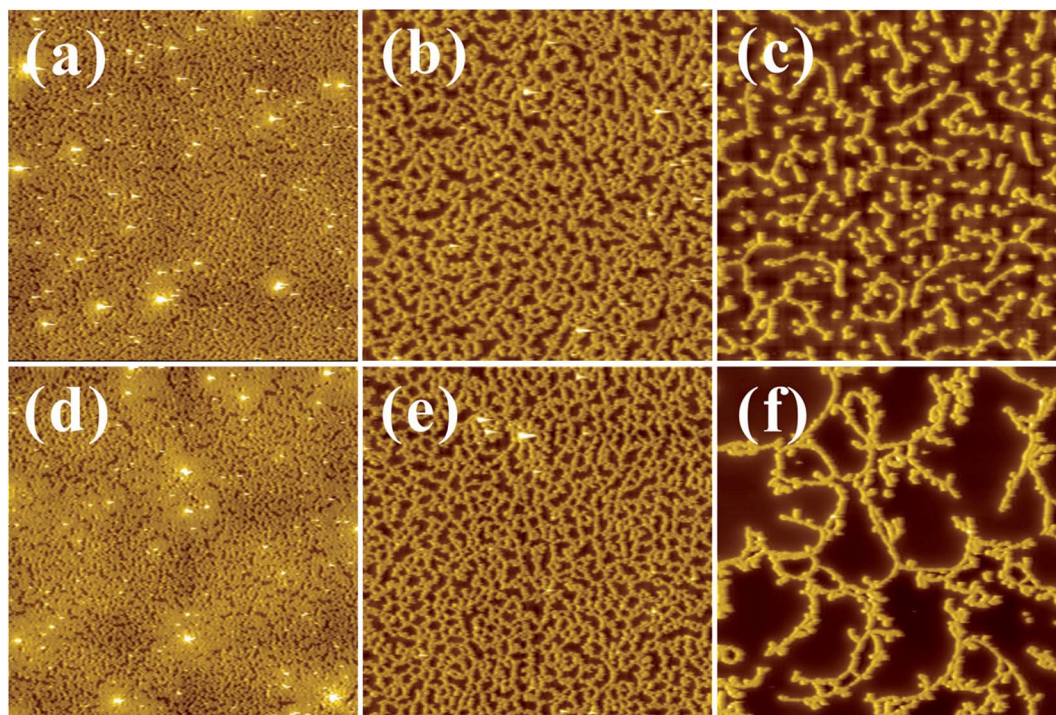

Fig. 4 AFM topography images (20 μm × 20 μm) of (a) S2VP[Eu(0.3)], (b) S2VP[Eu(0.5)], (c) S2VP[Eu(1.0)], (d) S2VP[Tb(0.3)], (e) S2VP[Tb(0.5)], and (f) S2VP[Tb(1.0)].

a strong driving force for autophobic dewetting because of the large reduction in conformational entropy in the wetting layer. Secondly, during evaporation of the deposited film, polymer chains underwent a marked change in conformation, from isolated individual coils to an entangled polymer film. Such non-equilibrated polymer chains might generate residual stresses within the film. Residual stresses are an extra driving force for dewetting, and are often at least the same order of magnitude as the acting capillary forces.[35] Any internal or external disturbances, such as heating, dust particles, film defects, or local mechanical forces acting on the film surface, provide a route for nucleation and the relaxation of residual stresses.[38] Furthermore, residual stresses arise from the strong biaxial constraint of the polymer film to the substrate. Attraction between Ln^{3+} and the pyridine groups in S2VP[Ln(x)] micelle cores could cause additional stress acting on the non-equilibrated polymer chains and certainly induce a stronger biaxial film constraint. Therefore, resulting from the complementary driving forces of autophobic behavior and residual stresses, S2VP[Ln(x)] film might rupture and dewet during the spin coating process. Furthermore, the driving force increased with increasing Ln^{3+} loading ratio, explaining the more obvious dewetting behavior at high Ln^{3+} concentrations (see Fig. 4).

In S4VP[Ln(x)], Ln^{3+} coordinated in micelle corona P4VP, as stated above. This association weakened the repulsive interactions between corona chains, resulting in stretching of the corona chain, which is not thought to induce significant residual stresses. Furthermore, although S4VP[Ln(x)] formed an anchored layer on substrate, no autophobic behavior appeared due to the different component in the top layer of anchored molecules (PS) and the corona of micelles (P4VP). Consequently, the addition of Ln^{3+} had no visible effect on S4VP film stability (Fig. SI-4†).

Photoluminescent properties of aggregates

Based on the different micelle structures of S4VP[Ln(x)] and S2VP[Ln(x)] mentioned above, their luminescence spectra were measured to explore the effect of Ln^{3+} distribution on luminescence efficiency. Fig. 5 depicts the emission spectra of S4VP[Eu(x)] and S2VP[Eu(x)]. Five characteristic emission peaks arose from transitions between the Russell–Saunders

multiplets, $^5D_0{}^7F_J$ (J = 0, 1, 2, 3, 4). The typical red color of the europium emission was mostly attributed to the strongest transition ($^5D_0{}^7F_2$), with a maximum intensity at 619 nm in our samples. The emission spectra of the Tb^{3+} complexes (Fig. 6) exhibited four main $^5D_4{}^7F_J$ transitions (J = 6, 5, 4, 3). The most intense peak, centered at 548 nm, was assigned to the $^5D_4{}^7F_5$ transition and was responsible for the pure green emission color. For all samples, the luminescent peaks did not show noticeable shifts in position. However, as shown in Fig. 7, the relatively intensities were significantly affected by the Ln^{3+} concentration and Ln^{3+} distribution (S2VP[Ln(x)] showed a higher emission intensity than S4VP[Ln(x)] at the same Ln^{3+} concentration).

The quantum yield of the luminescence step, Φ_{Ln}, expressed how well the radiative processes (characterized by rate constant k_r) competed with non-radiative processes (overall rate constant k_{nr}).

$$\Phi_{Ln} = \frac{k_r}{k_r + k_{nr}}$$

Contributions to k_{nr} included electron transfer quenching, back-energy transfer to the sensitizer, and, most importantly, quenching by matrix vibrations.[39] Therefore, to explain luminescence changes for various Ln^{3+} concentrations and distributions, three points should be considered: (i) interactions between Ln^{3+} and PVP segments; (ii) the isolation effect originating from the aggregate structure; and (iii) the changed Ln^{3+} coordination sphere.

As mentioned above, the pyridine rings in S2VP and S4VP can form strong coordination bonds with lanthanide ions, which were manifested from FTIR spectra (displayed above) and UV-vis absorption spectra (see Fig. SI-5†). With these coordination bonds, BCP served as an immobilization phase to form a stable rigid structure, which reduced the non-radiative vibronic deactivation (including vibrational and rotational energy transitions) of Ln^{3+} and resulted in higher energy transfer efficiencies.

The isolation effect of the aggregate structure was revealed by the stronger luminescent intensity of S2VP[Ln(x)] than S4VP [Ln(x)] at the same Ln^{3+} concentration. Deactivation of luminescence from excited Ln^{3+} in solution occurred by means of
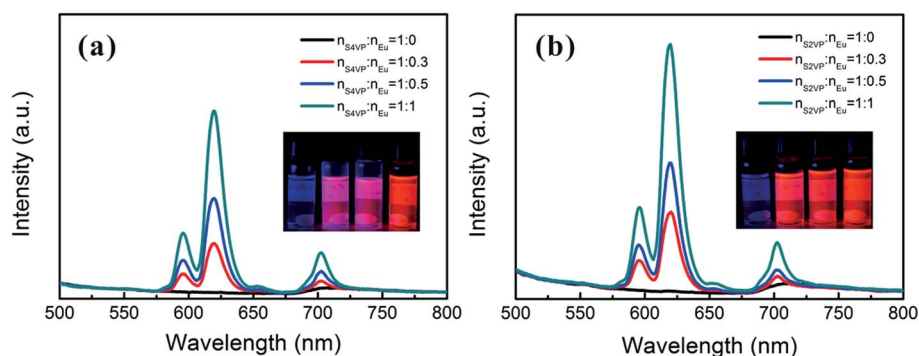

Fig. 5 Emission spectra of (a) S4VP[Eu(x)] and (b) S2VP[Eu(x)] with Eu^{3+} loading ratios ranging from 0 to 1.0.
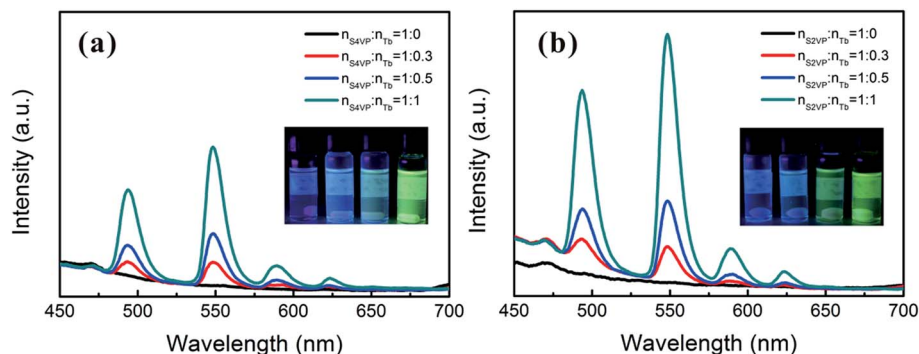
Fig. 6 Emission spectra of (a) S4VP[Tb(x)] and (b) S2VP[Tb(x)] with Tb^{3+} loading ratios ranging from 0 to 1.0.
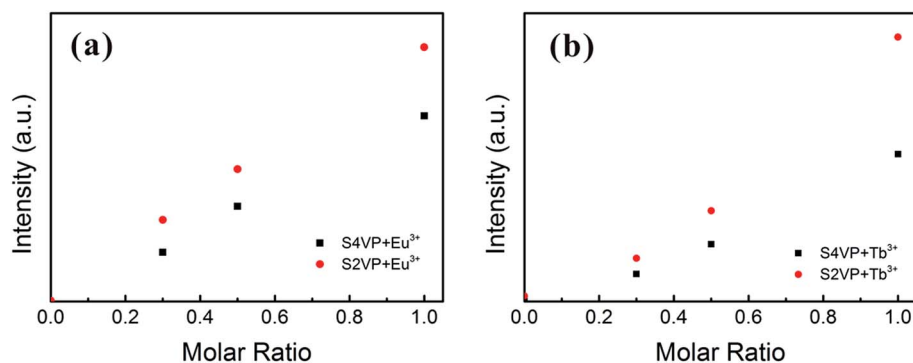

Fig. 7 Emission intensity of the (a) $^5D_0 \rightarrow ^7F_2$ peak of Eu^{3+} complexes and (b) $^5D_4 \rightarrow ^7F_5$ peak of Tb^{3+} complexes with increasing the Ln^{3+} concentration (molar ratio of Ln^{3+} ranging from 0 to 1.0).

a vibrational energy transfer process involving high-energy vibrations of solvent molecules or of bound ligands. Many investigations have shown that OH oscillators, such as those bound water or solvent alcohol molecules, were the most effective quenchers, both in the solid-state and solution. Therefore, the Ln^{3+} emission will be enhanced when Ln^{3+} is located in a relatively hydrophobic environment.[40,41] For S2VP [Ln(x)], the hydrophobicity of the exterior PS peripheries shielded quenching of excited Ln^{3+} and further reduced non-radiative deactivation.[17,42] Therefore, when the molar ratio of $n_{Ln^{3+}} : n_{VP}$ was fixed, S2VP[Ln(x)] presented a higher emission intensity than S4VP[Ln(x)].

In addition to the structural influences discussed above, the main factor affecting the luminescence property was the change in Ln^{3+} coordination spheres in complexes. The transitions of Ln^{3+} consisted mainly of magnetic dipole transitions and electric dipole transitions. Experimental data for the Ln^{3+} complexes indicated that the magnetic dipole transitions ($^5D_0 \rightarrow ^7F_1$ for Eu^{3+} and $^5D_4 \rightarrow ^7F_6$ for Tb^{3+}) were largely independent of the chemical surroundings of the ion. The electric dipole transitions ($^5D_0 \rightarrow ^7F_2$ for Eu^{3+} and $^5D_4 \rightarrow ^7F_5$ for Tb^{3+}), so-called hypersensitive transitions, are sensitive to the symmetry of the coordination sphere.[43] Therefore, the intensity ratio (η) of the magnetic dipole transition to the electric dipole transition in the lanthanide complex measured the symmetry of the coordination sphere.[43,44] High η value are known to denote

a high luminescent monochromaticity for different Ln^{3+} complexes, with Fig. 8 showing η values for different complexes. As shown in Fig. 8, the monochromaticity of both Eu^{3+} and Tb^{3+} increased with increasing Ln^{3+} concentration, showing that the presence of BCP generally increased the luminescent intensity of the hypersensitive transitions of Ln^{3+}. When Ln^{3+} was incorporated into the BCP micelles, the complexes exhibited disorder of a certain magnitude. The influences of PVP segments on the coordinative environment resulted in the polarization of Ln^{3+}, which changed the energy-transfer probabilities of the electric dipole transitions, accounting for the increase in luminescent intensity of the peaks at 619 and 548 nm for the Eu^{3+} and Tb^{3+} complexes, respectively. Moreover, S4VP[Ln(x)] presented a slightly higher η value than S2VP [Ln(x)], which could be explained by the symmetry of Ln^{3+} being more easily disrupted when Ln^{3+} was located in the micellar corona, due to Ln^{3+} being more likely to contact solvent molecules.

In short, under the cooperative influences of the three factors state above, the coordination of BCP on Ln^{3+} enhanced the luminescent efficiency of the Ln^{3+} complexes and protected them from quenching. Especially, when Ln^{3+} was associated within the micelle core, the protection effect of the hydrophobic shell distinctly enhanced the luminescence intensity.

Using the same procedure, samples were also prepared by the addition of 1 : 1 ($n_{Eu} : n_{Tb}$) lanthanide ions to a solution of
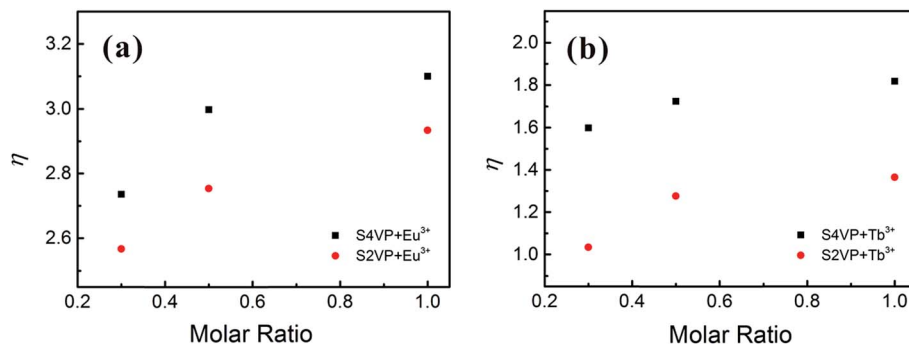
Fig. 8 Intensity ratio of the magnetic dipole transition to the electric dipole transition of (a) Eu^{3+} complexes and (b) Tb^{3+} complexes with increasing the Ln^{3+} concentration (molar ratio of Ln^{3+} ranging from 0.3 to 1.0).
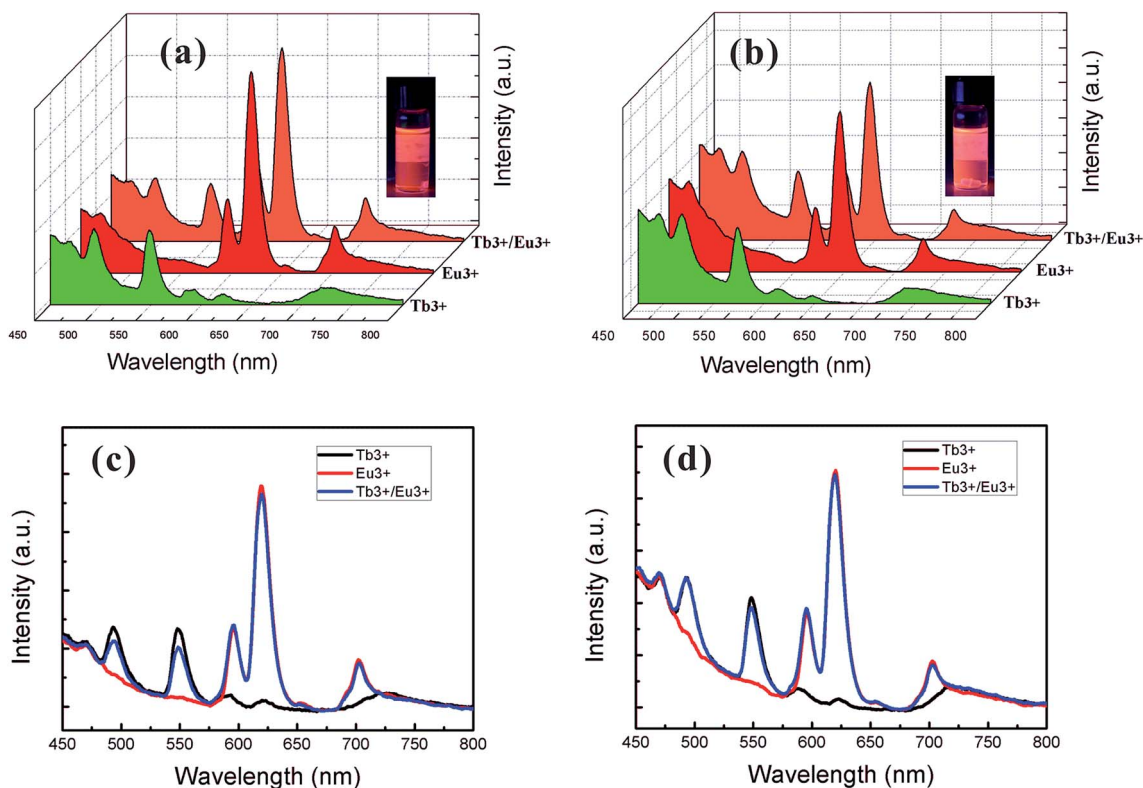

Fig. 9 Different views of emission spectra of (a, c) lanthanide ion/S4VP complexes and (b, d) lanthanide ion/S2VP complexes. Green, red and orange profiles correspond to Tb^{3+}, Eu^{3+}, and Tb^{3+}/Eu^{3+} complexes, respectively.

ion-free BCP, generating S4VP–$Eu_{0.5}Tb_{0.5}$ and S2VP–$Eu_{0.5}Tb_{0.5}$. The Eu–Tb compounds presented interesting luminescent properties. By mixing the appropriate combination of red and green light, orange emission was obtained. The emission spectra of the mixed samples gave addition spectra of the two chromophores (Fig. 9). The orange color was observed because Eu^{3+} is more emissive. This could be attributed to the possible energy transfer to the low-lying resonance state of Eu^{3+}, $^5D_0$ (17 300 cm^{-1}), from the $^5D_4$ of Tb^{3+} (20 400 cm^{-1}).[41] However, this possible energy transfer did not induce the total quenching of Tb^{3+}, which could be explained by the existence of three kinds of domains in the mixed complexes: two containing Eu^{3+} or

Tb^{3+}, and the third containing both Eu^{3+} and Tb^{3+}. Meanwhile, due to protection of the PS shell, S2VP–$Eu_{0.5}Tb_{0.5}$ presented a higher emission intensity than S4VP–$Eu_{0.5}Tb_{0.5}$.

Conclusions

In summary, the crucial role of Ln^{3+} ion distribution in micelles, thin films, and the photoluminescent properties of S4VP[Ln(x)] and S2VP[Ln(x)] were investigated in detail. The micelle size, film stability, and luminescent efficiency of these complexes were greatly affected by the Ln^{3+} ion distribution. With increasing Ln^{3+} concentration, S2VP[Ln(x)] micelles shrank and

films underwent autophobic dewetting due to coordination between Ln^{3+} and S2VP micelle core segments. In contrast, the S4VP[Ln(x)] micelle size increased and the films remained intact with the coordination of Ln^{3+} and micelle corona chains. Complexes containing Eu^{3+} and Tb^{3+} showed typical reddish and greenish luminescence that are characteristic of f–f transitions in lanthanide ions. The coordination of BCP to Ln^{3+} enhanced the luminescent efficiency and protected them from quenching. Especially when Ln^{3+} was located in the micelle cores, the exterior PS shells shielded quenching of excited Ln^{3+} and markedly enhanced the luminescent intensity of the complexes. Moreover, the emission spectra of mixed Eu–Tb ions complexes give addition spectra of the two separated complexes, resulting in an orange colored emission due to Eu^{3+} being more emissive. The results reported in this study may improve understanding of ion coordination and lay the foundation for applications of lanthanide ion/BCP complexes.

Author contributions

The manuscript was written with the contribution of all authors. All authors have given their approval to the final version of the manuscript.

Acknowledgements

References

1 T. P. Lodge, *Macromol. Chem. Phys.*, 2003, **204**, 265.
2 G. S. MacGlashan, Y. G. Andreev and P. G. Bruce, *Nature*, 1999, **398**, 792.
3 Z. Gadjourova, Y. G. Andreev, D. P. Tunstall and P. G. Bruce, *Nature*, 2001, **412**, 520.
4 R. P. Pereira, A. M. Rocco and C. Bielschowsky, *J. Phys. Chem. B*, 2004, **108**, 12677.
5 A. M. Christie, S. J. Lilley, E. Staunton, Y. G. Andreev and P. G. Bruce, *Nature*, 2005, **433**, 50.
6 N. Sabbatini, M. Guardigli and J. M. Lehn, *Coord. Chem. Rev.*, 1993, **123**, 201.
7 W. T. Carnall, P. R. Fields and K. J. Rajnak, *J. Chem. Phys.*, 1968, **49**, 4424.
8 J. C. Bünzli and C. Piguet, *Chem. Soc. Rev.*, 2005, **34**, 1048.
9 N. E. Wolff and R. J. Pressley, *Appl. Phys. Lett.*, 1963, **2**, 152.
10 Y. Ueba, E. Banks and Y. Okamoto, *J. Appl. Polym. Sci.*, 1980, **25**, 2007.
11 Y. Ueba, K. J. Zhu, E. Banks and Y. Okamoto, *J. Polym. Sci., Polym. Chem. Ed.*, 1982, **20**, 1271.
12 J. L. Bender, P. S. Corbin, C. L. Fraser, D. H. Metcalf, F. S. Richardson, E. L. Thomas and A. M. Urbas, *J. Am. Chem. Soc.*, 2002, **124**, 8526.
13 X. F. Qiao and B. Yan, *Inorg. Chem.*, 2009, **48**, 4714.
14 Y. Cong, J. Fu, Z. Cheng, J. Li, Y. Han and J. Lin, *J. Polym. Sci., Part B: Polym. Phys.*, 2005, **43**, 2181.
15 Z. Li, R. Ma, Y. An and L. Shi, *Colloid Polym. Sci.*, 2010, **288**, 1041.
16 Z. Li, R. Ma, A. Li, H. He, Y. An and L. Shi, *Colloid Polym. Sci.*, 2011, **289**, 1429.
17 Q. Xu, J. Tang, Y. Wang, J. Liu, X. Wang, Z. Huang, L. Huang, Y. Wang, W. Shen and L. A. Belfiore, *J. Colloid Interface Sci.*, 2013, **394**, 630.
18 D. H. Lee, S. H. Han, W. Joo, J. K. Kim and J. Huh, *Macromolecules*, 2008, **41**, 2577.
19 D. H. Lee, H. Y. Kim, J. K. Kim, J. Huh and D. Y. Ryu, *Macromolecules*, 2006, **39**, 2027.
20 F. Xue, H. Li, J. You, C. Lu, G. Reiter and S. Jiang, *Polymer*, 2014, **55**, 5801.
21 D. W. van Krevelen, *Properties of polymers: their correlation with chemical structure; their numerical estimation and prediction from additive group contributions*, Elsevier, 1990.
22 I. M. Smallwood, *Handbook of organic solvent properties: Amold*, 1996.
23 W. Zha, C. D. Han, D. H. Lee, S. H. Han, J. K. Kim, J. H. Kang and C. Park, *Macromolecules*, 2007, **40**, 2109.
24 H. Shen, L. Zhang and A. Eisenberg, *J. Am. Chem. Soc.*, 1999, **121**, 2728.
25 L. Zhang and A. Eisenberg, *Macromolecules*, 1996, **29**, 8805.
26 J. Meiners, A. Ritzi, M. Rafailovich, J. Sokolov, J. Mlynek and G. Krausch, *Appl. Phys. A: Mater. Sci. Process.*, 1995, **61**, 519.
27 G. Reiter, *Phys. Rev. Lett.*, 1992, **68**, 75.
28 A. Karim, N. Singh, M. Sikka, F. S. Bates, W. D. Dozier and G. P. Felcher, *J. Chem. Phys.*, 1994, **100**, 1620.
29 J.-U. Sommer and G. Reiter, in *Ordered Polymeric Nanostructures at Surfaces*, Springer, 2006, p. 1.
30 R. Limary and P. Green, *Langmuir*, 1999, **15**, 5617.
31 G. Reiter and R. Khanna, *Phys. Rev. Lett.*, 2000, **85**, 2753.
32 T. H. Epps, D. M. DeLongchamp, M. J. Fasolka, D. A. Fischer and E. L. Jablonski, *Langmuir*, 2007, **23**, 3355.
33 D. Yan, H. Huang, T. He and F. Zhang, *Langmuir*, 2011, **27**, 11973.
34 Y. S. Sun, S. W. Chien and J. Y. Liou, *Macromolecules*, 2010, **43**, 7250.
35 G. Reiter, M. Hamieh, P. Damman, S. Sclavons, S. Gabriele, T. Vilmin and E. Raphaël, *Nat. Mater.*, 2005, **4**, 754.
36 Y. Liu, M. Rafailovich, J. Sokolov, S. Schwarz, X. Zhong, A. Eisenberg, E. Kramer, B. Sauer and S. Satija, *Phys. Rev. Lett.*, 1994, **73**, 440.
37 G. Reiter, P. Auroy and L. Auvray, *Macromolecules*, 1996, **29**, 2150.
38 X. He, J. Winkel and W. T. S. Huck, *Adv. Mater.*, 2009, **21**, 2083.
39 M. H. Werts, R. T. Jukes and J. W. Verhoeven, *Phys. Chem. Chem. Phys.*, 2002, **4**, 1542.
40 W. D. Horrocks Jr and D. R. Sudnick, *J. Am. Chem. Soc.*, 1979, **101**, 334.
41 X.-P. Yang, C.-Y. Su, B.-S. Kang, X.-L. Feng, W.-L. Xiao and H.-Q. Liu, *J. Chem. Soc., Dalton Trans.*, 2000, 3253.
42 L. Xu, L. Feng, Y. Han, Y. Jing, Z. Xian, Z. Liu, J. Huang and Y. Yan, *Soft Matter*, 2014, **10**, 4686.
43 F. S. Richardson, *Chem. Rev.*, 1982, **82**, 541.
44 Q. Li, T. Li and J. Wu, *J. Phys. Chem. B*, 2001, **105**, 12293.